

# PHYSICAL REVIEW B

## CONDENSED MATTER

THIRD SERIES, VOLUME 31, NUMBER 7

1 APRIL 1985

### Measurement of positron reemission from thin single-crystal W(100) films

D. M. Chen,\* K. G. Lynn, R. Pareja,<sup>†</sup> and Bent Nielsen

*Physics Department, Brookhaven National Laboratory, Upton, New York 11973*

(Received 22 October 1984)

Epitaxial thin single-crystal (100) tungsten films 1000, 2500, and 5000 Å thick have been fabricated by high-vacuum electron-beam evaporation. These films were subsequently used as thin-film moderators for the study of the positron-transmission-reemission process with a variable-energy (0–80 keV) monoenergetic positron beam in an ultrahigh-vacuum system. The films were shown to be routinely cleanable by heating first in oxygen ( $10^{-6}$  Torr) and then in vacuum ( $10^{-9}$  Torr). Transmission and back reemission of slow positrons from these surfaces was observed. The positron work function,  $\phi_+$ , has been determined to be  $\approx 3.0$  eV ( $\pm 0.3$  eV). The transmission slow positrons were emitted in a narrow cone with a full width at half maximum of  $\approx 30^\circ$  consistent with the angular distribution of back-reemission positrons. The reemitted yields as a function of incident positron energy were found to be very different between forward reemission and back reemission. The maximum forward-reemission yields were 18% for 1000-Å-thick W film and 12% for 2500-Å-thick W film at 5 and 10 keV optimum incident positron energies, respectively. These results show that one can use thin single-crystal tungsten films as positron moderators or remoderators.

### INTRODUCTION

Slow-positron reemission from metal surfaces bombarded by high-energy positrons with a broad energy distribution has been utilized to develop narrow energy beams of slow positrons in the last decade.<sup>1</sup> The essential element of these beams is in most cases a moderator which is a well-annealed bulk metal (Cu, Ni, W, etc.). High-energy positrons created through  $\beta^+$  decay from a radioactive source ( $^{58}\text{Co}$ ,  $^{22}\text{Na}$ , etc.) are implanted into the moderator. They thermalize in  $\approx \frac{1}{100}$  of their bulk lifetime ( $\approx 200$  psec) and subsequently diffuse inside the crystal. A small fraction of them can return to the incident surface and be reemitted with a few electron volts of energy, a value characteristic of the negative positron work function. This moderation process will be referred to as “back reemission.” Another fraction of the thermalized positrons move deeper into the bulk and eventually annihilate inside the crystal. Clearly, one would expect to detect reemission from the opposite surface—if the moderator is sufficiently thin that some forward-diffusing positrons can reach this transmitting surface before they annihilate. This process will be called “forward reemission,” and the associated thin moderator, a “transmission moderator.” In addition to producing a narrow angular spread and small-energy-width positrons, moderators are also the basic elements for the attainment of a brightness-enhancement procedure realized by Mills.<sup>2</sup> The crucial parameter of moderators is their conversion efficiency

(number of slow positrons emitted versus the fast-positron flux), and, to a lesser extent, the angle and energy spread of the emitted positrons. At the present time, “back reemission” is the only geometry used for existing beams and the best overall moderator efficiency is about  $(2-3) \times 10^{-3}$ .<sup>3</sup> This efficiency has been increased by a factor of  $10^6$  since the discovery of this energy-moderation process in the 1950s.<sup>4</sup> Searching for high-conversion-efficiency moderators is still an important task for the development of slow-positron physics.

One of the disadvantages of the back reemission moderator is that a significant fraction of the moderated positrons are recaptured by the source cross section ( $\approx 20\%$  for a needle source)<sup>3</sup> on their drift path from the moderator, known as the “source-shadow” problem. It is this problem that seriously restricts the present use of the  $^{22}\text{Na}$  source,<sup>5</sup> although it has a long half-lifetime (2.6 y) and a high  $\beta^+$ -decay fraction (90%) and can now be made in a high-specific-activity form ( $\approx 600$  Ci/gm). Another problem associated with the back-reemission geometry arises in the application of remoderation to produce a brightness-enhanced beam. Since slow positrons are reemitted in a narrow cone centered along the normal direction of the incident surface, a sophisticated configuration of the electromagnetic field is necessary to produce remoderation. In contrast, such problems do not exist for transmission moderation, because the source is on one side of the moderator and the transmitted reemitted positrons are on the other. In these respects a transmission modera-

tor should be a good improvement for this energy-moderation process and would allow simplification in most optical configurations for multiple remoderation. These transmission moderators should also produce a highly polarized slow-positron beam.<sup>6</sup> In this paper we will present our experimental and theoretical results on the reemission of positrons from single-crystal tungsten thin films.

### EXPERIMENTAL DETAILS

The positron-reemission measurements were performed using a variable-energy positron beam. The incident-positron energy can be varied from 0 to 80 keV. The moderated positrons are transported by an axial magnetic guiding field generated by a number of solenoid coils.<sup>7</sup> Figure 1 is the schematic of our apparatus in the target region. The measurement system is housed in an ultrahigh-vacuum chamber.

In this design two  $\mathbf{E} \times \mathbf{B}$  energy analyzers are installed, one on each side of the thin film. Back reemission as well as forward reemission can be studied simultaneously or separately. The basic components of the analyzer are a set of parallel plates and a channel electron multiplier (CEM) mounted at one end of the plates with an offset from the initial beam path. Also attached to the analyzers are acceleration (ACC) plates. They attract the back-reemitted and forward-reemitted positrons into the  $\mathbf{E} \times \mathbf{B}$  analyzers. The analyzer plates are parallel to the guiding  $\mathbf{B}$  field, providing a transverse  $\mathbf{E}$  field. As a consequence of this crossed static electromagnetic field, slow positrons are deflected a distance according to the axial component of their momentum. Fast positrons are negligibly affected. The collimator in front of the CEM determines a window, and only positrons with the corresponding energy are

detected. By sweeping the reemitted-positron energy (e.g., the sample bias), a differential energy spectrum can be obtained. The energy resolution of the analyzer depends on its geometry,  $\mathbf{B}$  field, and the collimator size. The finite angular spread of the reemitted positron also reduces the energy resolution. In our measurements, the difference in the plate voltage was 7 V, and the total width of the elastic peak was about 180 meV as measured with a Ni(111) single crystal in which approximately 70 meV is from the intrinsic positron width.<sup>7</sup> When the pass energy is held fixed, these analyzers can be used to measure the positron work function, angular distribution, and the relative reemission yield for different incident-positron energies. The symmetry of the configuration in the first section of the chamber also plays a useful role in removing the systematics of our measurements. For example, the forward-reemitted positrons are deflected into analyzer 2 and have no chance to return to the sample region, or into the other analyzer, which detects the back-reemitted positrons. The same is true for analyzer 1.

In addition, a NaI(Tl)  $\gamma$ -ray detector was utilized to measure the integral reemission yields and the positronium fraction by established procedures.<sup>8</sup> The NaI detector was perpendicular to the beam path, approximately 10 cm away from the center of the thin-film sample, and was shielded with a lead collimator. This orientation was selected to limit the detector's solid angle and eliminate the signal contributed by the positrons annihilating in the  $\mathbf{E} \times \mathbf{B}$  detectors, as well as other unwanted annihilations. Voltage was also applied on the ACC plates and the analyzer plates to ensure that only forward- or back-reemitted positrons were studied at any one time with the NaI(Tl) detector. For the data taken with the NaI(Tl) detector, no corrections were made for annihilations in the grid or for a solid angle.<sup>9</sup>

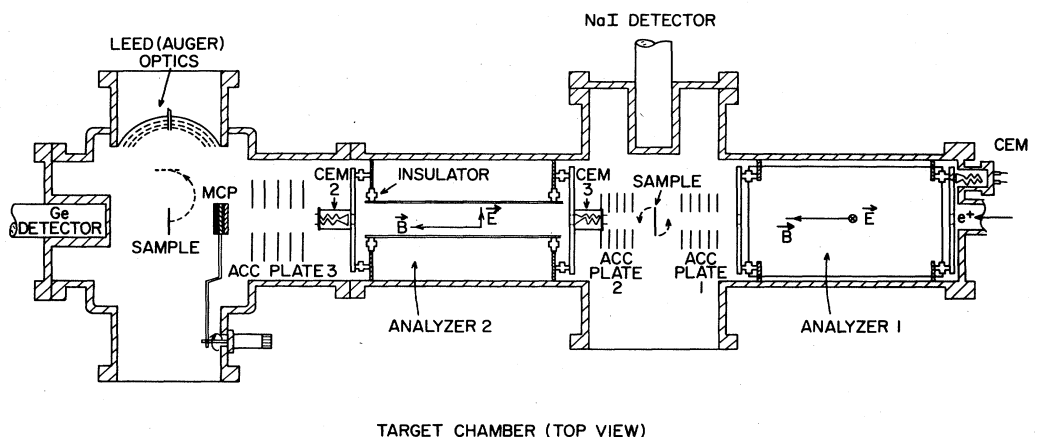


FIG. 1. Schematic view of the target chamber. Reemitted positrons from either sample can be studied by using this configuration. The thin-film samples are inserted between accelerator plates 1 and 2 and can be rotated both for angular studies as well as testing each surface in both forward and backward directions. The channel electron multiplier array labeled MCP can be moved into the beam position to examine the beam profile as well as the nonthermals transmitted through the thin film. A collimator is also installed in the beam before it enters the target chamber. Four different thin films can be inserted by using our sample manipulator.

### FILM PREPARATION

In principle, to achieve transmission moderation with an incident beam of fast monoenergetic positrons, the thickness of the moderator should be on the order of the sum of the positron mean implantation depth and diffusion length in the moderator. For our beam capability, and other reasons which will be discussed later, moderators as thin as few  $10^3$  Å were necessary. One of the crucial technical steps for this experiment is, therefore, to fabricate high-quality (i.e., low defect concentrations), cleanable, self-supporting, single-crystal, thin metal films. It has been reported by Vehanen *et al.*<sup>3</sup> that, in case of back reemission, the W(110) moderator provides the highest conversion efficiency among the materials tested to date. Therefore, W films were chosen for fabrication in a thin-film configuration.

An electron-evaporation technique similar to that of Mertler *et al.*<sup>10</sup> was used to produce these films. Initially, a large-mosaic-spread ( $\approx 10^\circ$ ) molybdenum single crystal was grown on a MgO(100) host substrate, and this composite served as the substrate for the tungsten film. In this experiment,  $25 \times 25$  mm<sup>2</sup> crystals, 1 mm thick, cleaved in air along the (100) crystal plane, were used as primary substrates. The unpolished substrate was mounted on a Ta holder which maintained the substrate temperature at  $\approx 1000^\circ\text{C}$ , while Mo and W were deposited sequentially onto the substrate with a deposition rate of 6 Å/s. Both the Mo and W layers were expected to have (100) orientation. The vacuum was kept between  $1 \times 10^{-7}$  and  $5 \times 10^{-7}$  Torr during the evaporation. Earlier films grown under a pressure in the high- $10^{-6}$ -Torr range in a different vacuum system were also found to be small-mosaic-spread single crystals. The thickness of the Mo layer was  $\approx 2000$  Å. The W-film thicknesses varied between 1000 and 5000 Å. The film thicknesses were determined *in situ* by water-cooled rate monitor near the substrate. However, these thicknesses could change, especially after removal of the film from the substrate and subsequent surface-cleaning procedures.

To obtain the self-supporting W films, a 80 vol %  $\text{H}_2\text{PO}_4$  and 20 vol %  $\text{H}_2\text{O}$  solution at  $90^\circ\text{C}$  was used to dissolve the MgO crystal. The Mo layer was removed thereafter by etching in a solution consisting of 45 vol %  $\text{H}_2\text{SO}_4$ , 25 vol %  $\text{HNO}_3$ , and 30 vol %  $\text{H}_2\text{O}$  at  $70$ – $90^\circ\text{C}$ . Finally, some of the W films so obtained were investigated by transmission x-rays techniques. Others were investigated by transmission electron microscopy (TEM). The x-ray and TEM results confirmed that they were (100)-oriented single-crystal W films.

The W film was placed between a folded 95% transmission W mesh, which also served as the sample heater. Before the films exhibited good positron-diffusion characteristics consistent with a defect-free film, the samples had to be heated above  $1800^\circ\text{C}$  under high vacuum ( $\approx 10^{-9}$  Torr). This positron-diffusion length was determined by measuring the emitted positronium (Ps) fraction versus incident-positron energy. The removal of positron-trapping centers (i.e., open-volume defects) is essential for a long positron-diffusion length, i.e., high-conversion-efficiency moderator.

Positron-reemission properties also strongly depend on the surface condition.<sup>1</sup> This, in turn, enabled us to determine, to a good extent, the surface condition by means of the positron-reemission differential spectrum, even though low-energy electron-diffraction (LEED) and Auger-electron spectroscopies were not available in this section of the system. In general, surface treatment, e.g., removal of the surface contaminant, is required before a high positron-reemission yield can be obtained. For tungsten, carbon is believed to be the dominant impurity, and heating in oxygen followed by an annealing procedure was found to be effective in reducing carbon and other surface contaminants.<sup>11</sup> Because of the fragility of the W films the procedure was as follows: After the vacuum pressure reached better than  $10^{-9}$  Torr, the films were treated first by heating in oxygen ( $\approx 10^{-7}$  Torr) at  $700$ – $800^\circ\text{C}$  for 40 min and then in vacuum ( $10^{-9}$  Torr) at  $2000^\circ\text{C}$  for 1 min. This procedure was repeated ( $\approx 3$  or 4 cycles) until the films showed good positron-reemission properties.

To illustrate the results of this method, two plots of the differential energy spectrum of the forward-reemission positions for different cleaning results are presented in Fig. 2. The peaks are normalized for the comparison of the right-hand shoulders of the peaks.<sup>8</sup> These shoulders

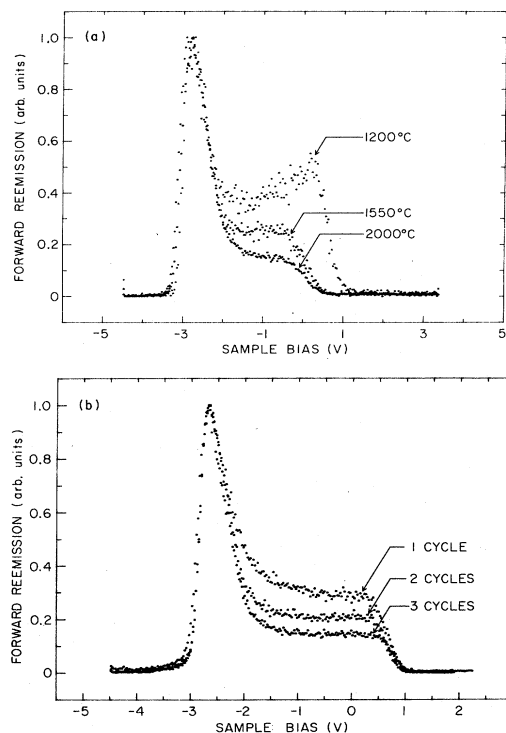


FIG. 2. (a) Forward-reemitted positron differential energy spectrum taken for 2500-Å-thick W(100) film bombarded with 12-keV incident positrons after two cleaning cycles. The film was heated in oxygen first and then heated to different temperatures as indicated in the figure. (b) Differential energy spectrum of the forward-reemitted positrons from 1000-Å-thick W(100) film bombarded with 5.85-keV incident positrons. Spectra were taken after different number of sample-cleaning cycles.

are produced by positrons from the surface which experience inelastic or elastic scattering from electrons and phonons as well as microscopic roughness. The latter effect changes the angle of emission; thus the axial component of the momentum, which is the quantity measured, is changed. The peak-to-shoulder ratio, together with the total yield and work function, provides knowledge of the film.<sup>1</sup> Figure 2a shows the results of heating the film to the various temperatures after cleaning in O<sub>2</sub>. The overlayer of oxygen is responsible for the large change in the scattered fraction ( $T \leq 1200^\circ\text{C}$ ) and for the increase of the work function as well as increase the total reemission yield.<sup>11</sup> Figure 2(b) indicates that more than two cleaning cycles are needed in order to reduce the scattered fraction. It should be noted that this procedure is not unique. For a film mounted between molybdenum rings with an  $e^-$  gun as a heating source, it was found that direct heating in the vacuum was sufficient for good reemission properties. Unfortunately, damage to the film associated with thermal stress was the serious problem for this mounting. The discrepancy suggests, perhaps, that the W mesh was the major donor of the carbon impurity on the surfaces of the film. Therefore it is suggested that the mesh be degassed to remove the carbon from it prior to film mounting.

## RESULTS AND DISCUSSION

Both the back- and forward-reemitted positrons possess the same characteristics, i.e., small energy spread and narrow beam emission. The most direct method of exploring these features is measurement of the differential or integral positron-energy spectrum and the angular distribution of the reemitted positrons.

Typical examples of the measured differential energy spectra are shown in Fig. 3 for the  $\approx 2500\text{-}\text{\AA}$ -thick film with an incident-positron energy of 12 keV. Again, the peak has been normalized for ease of comparison. In Fig. 3(a) two spectra of reemitted positrons are shown from the same surface, one in back reemission and one in forward reemission. The back-reemission spectrum had to be shifted by 0.15 V to make the two peaks coincide. The shift, as well as the slight deviation along the shoulders, is attributable to differences in the characteristics of the analyzers. In Fig. 3(b) both spectra are for forward reemission, one for each side of the film surfaces. Their coincidence shows that identical surface conditions are obtainable. The positron work function ( $\phi_+$ ) can easily be deduced from these spectra by determining the difference in the voltage where the peak maximum occurs and the half-value after the plateau.<sup>1</sup> It is important to see that the forward-reemitted positrons have the same energy as the back-reemitted positrons; the value of  $\phi_+$  is  $\approx -3.0$  ( $\pm 0.3$ ) eV, consistent with Refs. 3 and 11. The same value was also extracted from the integral energy spectrum measured with the NaI(Tl) detector and from similar measurements for 1000- and 5000- $\text{\AA}$ -thick W films. The error bars associated with  $\phi_+$  arise from three factors: (1) the  $\mathbf{E} \times \mathbf{B}$  energy analyzer had a total width of 180 meV, (2) the peak position of the differential spectrum changes appreciably as the normal direction of the

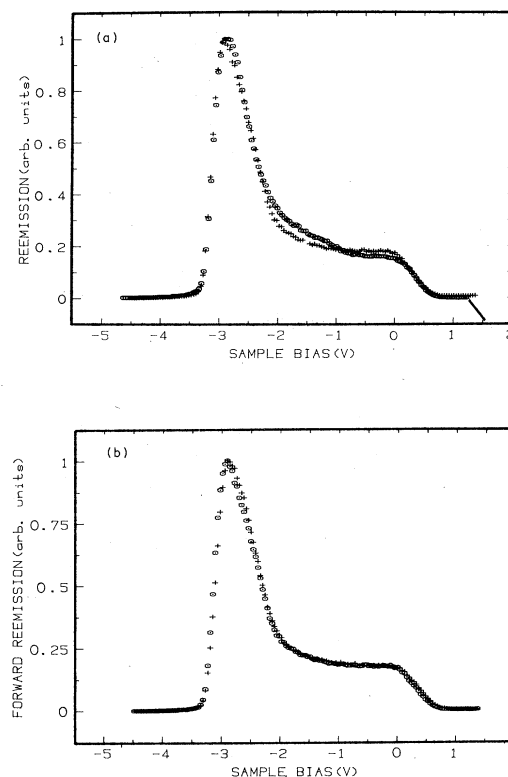


FIG. 3. Differential spectra are shown for the  $\approx 2500\text{-}\text{\AA}$ -thick W(100) thin film after a number of cleaning cycles. The spectra have been peak-normalized for ease in comparison. The incident-positron energy was 12 keV. (a) The forward and back reemission spectra represented by + and o, respectively, were taken simultaneously. The back-reemission spectrum was shifted by  $-0.15$  V to align the two peaks. This energy shift is attributable to the difference in the geometry and contact potential between the analyzer systems. The positron work function ( $\phi_+$ ) can be measured from the peak maximum ( $-2.8$  V) to the decrease to zero counts at  $\approx 0.2$  V. Therefore the work function in this case is approximately  $-3.0$  V (Ref. 4). (b) Forward reemission energy differential spectra for both sides of the film are shown with different symbols. It is worth noting that the nonthermal fraction (left shoulders of the peaks) plays only a minor role in these measured spectra.

emission surface deviates from the beam axis<sup>8</sup> [Fig. 4(a)], and (3) the angular spread of the reemitted positrons increases the measured width because only the axial component of the momentum is selected. A more accurate work-function measurement should be performed with a thicker sample and a crystal that has been well characterized for comparison of these films.

The forward-reemission angular distribution curves for a 1000- $\text{\AA}$ -thick film with 5 keV incident-positron energy are shown in Fig. 4. In Fig. 4(a) the differential energy spectra were taken for constant run time as the normal direction of the sample relative to the beam axis was rotated  $0^\circ$ ,  $15^\circ$ , and  $30^\circ$ . The peak counts are plotted versus sample angle in Fig. 4(b). It should be realized that as the

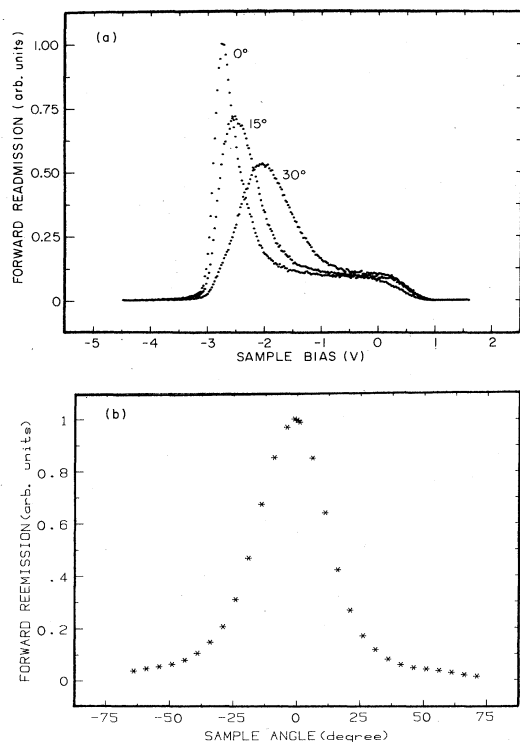


FIG. 4. (a) Differential energy spectra of the forward-remission positrons with the normal direction of the film rotated through angles of 0°, 15°, and 30°, respectively, relative to the beam axis. The film thickness was 1000 Å and the incident-positron energy was 5 keV. (b) Angular distribution of the forward-remission positrons from a 1000-Å-thick W(100) film with 5-keV incident-positron energy. The limitation of the energy resolution of the  $E \times B$  detector slightly broadened this "bell-shaped" spectrum.

sample is rotated an angle  $\theta$ , the effective thickness "seen" by the incident positrons increases, and the mean implantation depth at the same energy decreases. Furthermore, the backscattering probability from the incident surface increases slightly as  $\theta$  increases.<sup>12</sup> However, our measurements are not able to demonstrate this small effect because of the limited energy and angular resolution as well as the imperfect film (pin holes and surface roughness). Nevertheless, the shift of the peak position in Fig. 4(a) is a pure effect of the small angular spread of reemitted positrons and should follow a  $\cos^2\theta$  result. Qualitatively, these results are in good agreement with those reported for the back-reemitted positrons.<sup>8</sup> The above evidence proves unambiguously the existence of the transmission reemission process.

Besides the similarities between forward and back re-emission, the forward- and backward-reemission yields change very differently as a function of the incident-positron energy. In Fig. 5 the forward-, backward-, and total-reemission yields are shown as determined by the NaI(Tl) detector for the 2500-Å-thick W film. Figure 6 shows forward-reemission yield versus incident-positron energy as measured by the  $E \times B$  detector with the win-

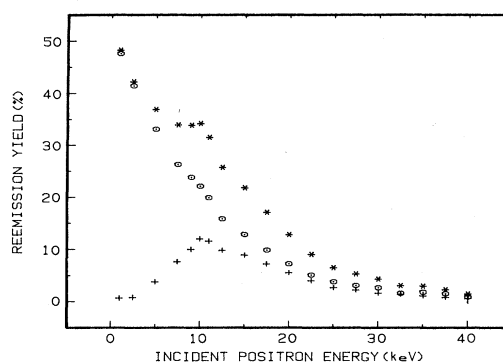


FIG. 5. Total-, forward-, and backward-reemission yields as determined by the NaI(Tl) detector measured for the 2500-Å-thick W(100) film at various incident energies. No correction has been made for the background or grid annihilations. + forward reemission; o, back reemission; \*, total reemission.

dow set for the peak count. One can see good agreement between the general shape of the curves. However, the transmission efficiency of the analyzer has not been determined. With our present beam, the beam spot oscillates as a function of incident energy, which changes the transmission efficiency of the analyzer. These oscillations were removed by smoothing the curve in Fig. 6. Unlike the monotonic decay of the back-reemission yield, the forward-reemission yield increases as the incident energy increases from zero, reaches its maximum value, and subsequently decreases. The maximum values of the forward-reemission yield are 18% for the 1000-Å-thick W film and 12% for the 2500-Å-thick W film (Figs. 5 and 7). The corresponding incident-positron energies are  $\approx 5$  and  $\approx 10$  keV, respectively. The ratios of the maximum yield in backward reemission to the maximum in forward reemission are about 2.6 for the 1000-Å-thick film and 4 for the 2500-Å-thick film. The total-reemission yield is the sum of the forward- and back-reemission yields. It maintains a high value over the approximately 5-keV en-

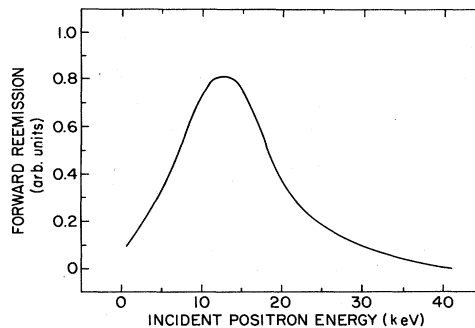


FIG. 6. Forward reemission yield as measured by analyzer 2 at various incident-positron energies. The curve has been modified to remove oscillations which are associated with the beam movement at various incident-positron energies. One can see that the maximum which occurs around 13 keV is in agreement with that in the preceding figure.

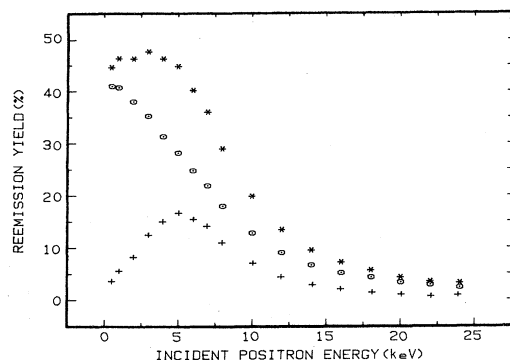


FIG. 7. Total-, forward-, and backward-reemission yields as determined by the NaI(Tl) detector measured for the  $\approx 1000$ -Å-thick W(100) film vs incident-positron energy. No correction has been made for the background or grid annihilations. The maximum was about 18% for 5-keV incident-energy positrons. +, forward reemission; o, back reemission; \*, total reemission.

ergy range for the 1000-Å-thick film (Fig. 7), a special feature neither the back- nor the forward-reemission yields possess.

The forward-reemission yield is also a function of the positron mean implantation depth, the film thickness, and the type of material under study. Ideally, it would be preferable to implant the positrons very close to the transmitting surface. Unfortunately, the actual positron-implantation profile sets limitations for this application because the profile broadens rapidly as the incident energy increases.<sup>13</sup> When the mean implantation depth approaches the transmitting surface of the film, a significant number of positrons will pass through the film before they are completely thermalized. Nevertheless, for low incident energy, the profile is rather localized. Low incident-positron energy, very thin, and high-atomic-number films are, therefore, theoretically preferred for a high-yield transmission remoderator. For each selected film and thickness there exists an optimum value of the incident energy which maximizes the forward-reemission yield or vice versa. This argument is true only for the monoenergetic incident beam, i.e., for the remoderation process. For a primary moderator, positrons created through  $\beta^+$  decay from radioactive sources have a wide energy distribution (i.e.,  $\beta^+$  spectrum), and the forward-reemission yield in this case is the convolution of the emitted  $\beta^+$  spectrum with the yield as a function of energy for a particular moderator [Eq. (A14)].

At the present time three different film thicknesses have been examined, namely 1000, 2500, and 5000 Å. The films have been cleaned and exhibited good reemission properties. These results have also been compared to theory (i.e., diffusion model) and appear to be in general agreement. Comparison between theory and data is briefly discussed in the Appendix.

In conclusion, it has been shown that one can produce thin single-crystal W(100) films capable of reemitting positrons at a sufficiently high fraction to be used either as a transmission moderator or as a remoderator. Both the impurities and defects can be removed by the appropriate

cleaning and annealing procedures, and narrow-beam emission was attained when the films were cleaned.

Another effective way of utilizing these thin-film moderators is to collect both the back- and forward-reemission positrons and to bring them together. The electromagnetic field configuration will be the major concern for this purpose. To make further use of the non-thermalized transmitting positrons, multiple thin films can be installed. From the results of this experiment, we suggest that further studies should be carried out for films made up of different materials (Ni, Cu, Mo, etc.) as well as films with interfaces comprised of two different materials for which positron work functions have the opposite sign or different values. The forbidden or reduced reemission of positrons from one surface (positron diode) should enhance the reemission yield from another surface. This technique should also be useful for characterizing defect concentration at interfaces or in thin films.

## ACKNOWLEDGMENTS

We would like to thank J. Hurst and M. Carroll for technical assistance in this project, M. Strongin and the Massachusetts Institute of Technology for the use of their vacuum system where some of the thin films were grown, and A. Mills for continued discussions. This research was supported by the Division of Materials Sciences, U. S. Department of Energy, under Contract No. DE-AC02-76CH00016 and, in part, by the National Science Foundation through Grant No. DMR-83-15691.

## APPENDIX

### Theoretical analysis

The motion of thermalized positrons in bulk materials can be well described by a one-dimensional diffusion model, i.e., the one-dimensional diffusion equation alone with some appropriate boundary condition and an initial condition (implantation profile). Successful results of comparisons between theoretical calculations and experiments for thick bulk materials can be found in the literature.<sup>14,15</sup> Lynn and Wachs used this model to calculate properties of thin Cu and Si ( $\approx 1 \mu\text{m}$ ) foils and obtained some numerical solutions for a perfect-absorption boundary condition and an exponential implantation profile.<sup>16</sup> Recently, from their Monte Carlo calculation, Valkealahti and Nieminen suggested a better representation of the positron-implantation profile.<sup>13</sup> Adapting their new profile, the model can be expressed as

$$\frac{\partial n(x,t)}{\partial t} = D_+ \frac{\partial^2 n(x,t)}{\partial x^2} - \lambda n(x,t), \quad (\text{A1})$$

$$n(o,t) = n(T,t) = 0, \quad (\text{A2})$$

$$n(x,o) = P(x) = \frac{mx_0^{m-1}}{x_0^m} \exp[-(x/x_0)^m], \quad (\text{A3})$$

where  $n(x,t)$  is the positron-density distribution in the thin film,  $T$  is the film thickness,  $x=o$  and  $x=T$  denote the two surfaces of the film, and  $D_+$  and  $\lambda$  are the positron-diffusion coefficient and disappearance rate (i.e.,

bulk annihilation rate and defect-trapping rate), respectively. For a well-annealed single crystal, the defect-trapping rate is negligible and  $D_+$  as well as  $\lambda$  can be considered to be constants.

Equation (A2) implies a "perfect-absorption" boundary condition, namely an infinite probability of removing positrons from the surface. There are three escape mechanisms to which positrons reaching a surface are subject:<sup>15</sup>

(1) the formation of positronium and escape into the vacuum, (2) becoming bound in the positron surface state, and (3) reemission as slow positrons. It has also been suggested in Ref. 15 that thermal positrons at low temperatures are strongly reflected from the surface. To take this effect into account, a radiative boundary condition must be used. Because of the relatively high branching ratio ( $B$ ) of slow-positron reemission, only the perfect-absorption boundary condition was used in our calculation; however, inclusion of this term would not change our conclusions.

In Eq. (A3),  $x_0$  is related to the mean implantation depth  $\bar{x}$  according to

$$\bar{x} = x_0 \Gamma(1 + 1/m), \quad (\text{A4})$$

where the  $\Gamma$  function is a function of  $m$ , which is the shape parameter. The value of  $m$  was found in Ref. 13 to be approximately 1.9 for "semi-infinite" Al, Si, Cu, and Au. The empirical formula of the energy dependence of  $\bar{x}$  is

$$\bar{x} = AE^n, \quad (\text{A5})$$

where  $E$  is the incident-positron energy;  $A$  and  $n$  are parameters determined by experiments and their values for several materials are summarized in Table II of Ref. 13. The implantation profile (A3) is area-normalized in the semispace, i.e.,  $\int_0^\infty P(x)dx = 1$ . This means that the fraction of positrons,  $\int_0^T P(x)dx$ , will pass through the film before it is completely thermalized, and only the remaining fraction,  $\int_0^T P(x)dx$ , will be stopped inside the film. As one increases the incident energy, the stopping fraction becomes smaller. This effect is pronounced when the mean implantation depth  $\bar{x}$  approaches and crosses the transmitting surface.

The forward-reemission yield  $Y_F$ , the back-reemission yield  $Y_B$ , and the current density  $j(x, t)$  can be derived immediately from the positron density distribution:

$$Y_F(E) = B \int_0^\infty j(T, t) dt, \quad (\text{A6})$$

$$Y_B(E) = -B \int_0^\infty j(0, t) dt, \quad (\text{A7})$$

$$j(x, t) = -D_+ \frac{\partial n(x, t)}{\partial t}. \quad (\text{A8})$$

Or upon solving Eqs. (A1)–(A3),

$$Y_{B,F} = B \int_0^T G_{B,F}(T, x) P(x) dx, \quad (\text{A9})$$

where  $B$  is the branching ratio of reemission. The Green's functions were found to be

$$G_B(T, x) = \frac{\sinh[(T-x)/L_+]}{\sinh(T/L_+)}, \quad (\text{A10})$$

$$G_F(T, x) = \frac{\sinh(x/L_+)}{\sinh(T/L_+)}, \quad (\text{A11})$$

where  $L_+ = (D_+/\lambda)^{1/2}$  is the positron diffusion length. Note that Eqs. (A9)–(A11) are, as expected, the same as the solution of stationary diffusion model,<sup>17</sup> another way of describing the same problem.

With a change of variables,  $Y_B$  and  $Y_F$  are functions of two dimensionless parameters  $\alpha$  and  $\eta$  which are defined as  $\alpha = T/L_+$  and  $\eta = (E/E_0)^n/\Gamma(1 + 1/m)$ , where  $E_0^n = L_+/A$ . The final equations become

$$Y_F = \frac{1}{\sinh(\alpha)} \int_0^\alpha \sinh(x) \frac{mx^{m-1}}{\eta^m} \exp[-(x/\eta)^m] dx, \quad (\text{A12})$$

$$Y_B = \frac{1}{\sinh(\alpha)} \int_0^\alpha \sinh(\alpha-x) \frac{mx^{m-1}}{\eta^m} \exp[-(x/\eta)^m] dx. \quad (\text{A13})$$

Thus only the ratio of the film thickness to the diffusion length plays an important role. Apart from the  $\Gamma$  function, the incident energy is "normalized" in a manner identical to that in the case of thick materials.<sup>14,16</sup>

We have fitted Eqs. (A12) and (A13) to our yield-measurement data (Figs. 5 and 7), leaving  $n$ ,  $m$ ,  $E_0$ ,  $\alpha$ , and  $B$  as floating parameters. Two constraints were imposed: (a)  $n$  and  $m$  must be the same for both films, and (b)  $E_0$ ,  $\alpha$ , and  $B$  must be the same for  $Y_B$  and  $Y_F$  of each film. For this reason, these four sets of data were fitted simultaneously. The fitting results with reasonable parameters are shown in Figs. 8 and 9, and in Table I.

In order to save the films for the future experiments, we were not able to measure the final thicknesses of these films. With the initial estimated thicknesses and the obtained values of  $\alpha$ , the definition of  $\alpha$  leads to  $L_+ = 1377$  and  $1381$  Å, respectively. The ratio of two  $\alpha$  values is 2.49, consistent with the ratio of the estimated thicknesses (2.5). The inequality of the branching ratios can be interpreted as being due to the different surface conditions. The differences between the experimental data and the fittings are attributable to the following:<sup>17,18</sup>

(1) Some fast positrons were backscattered from the incident surface.<sup>12</sup> These particles are not deflected a signi-

TABLE I. Fitted parameters for  $Y_F$  and  $Y_B$  [see Eqs. (A12) and (A13)] to the yield-measurement data for 1000- and 2500-Å-thick W(100) films.

Estimated $T$ (Å)	$n$	$m$	$\alpha = T/L_+$	$E_0$ (keV)	$B$
1000	1.80	1.14	0.726	9.00	51.2
2500	1.80	1.14	1.81	10.6	44.5

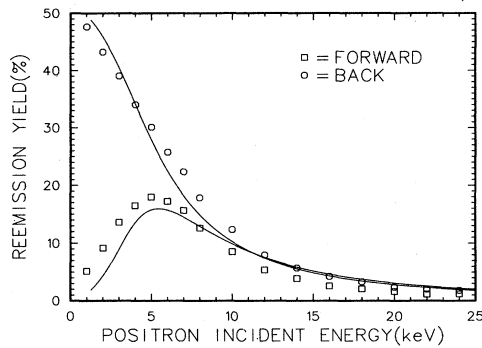


FIG. 8. Data and fit for the 1000-Å-thick W film are shown. The solid curves are generated from the theoretical expressions with fitted values as listed in Table I.

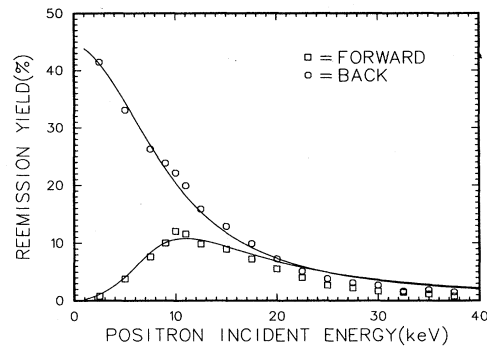


FIG. 9. Data and fit for the 2500-Å-thick W film. The solid curves are generated from the theoretical expressions [Eqs. (A12) and (A13)] with fitting parameters given in Table I.

ficant amount by the  $\mathbf{E} \times \mathbf{B}$  analyzer because they only spend very little time in the analyzer region. After being reflected by the beam accelerator, they again arrive at the film. This will change the implantation-profile parameter  $m$ .

(2) The transmitting surface will modify the implantation profile in its neighborhood.

(3) The internal reflection of diffusing positrons has not been taken into account since only the perfect absorption boundary condition was considered.

Knowing the yields as a function of incident-positron

energy and the film thickness, the above derivation can easily be extended to obtain the total yield for a primary moderator,

$$Y_{B,F}(T) = \int_0^{E_{\max}} \beta(E) Y_{B,F}(E, T) dE, \quad (\text{A14})$$

where  $\beta(E)$  is the energy distribution of  $\beta$ -decay positrons from some isotope. Even with this simple model, Eq. (A14) should give, to a reasonable degree, a relation between the yield and the moderator thickness, an important result for the design of slow-positron beams.

\*Permanent address: City College of New York, NY 10031.

†Permanent address: Universidad Complutense, Facultad de C. Fisicas, Departamento Estado Solido, Madrid-3, Spain.

<sup>1</sup>A. P. Mills, Jr., in *Proceedings of the International School of Physics "Enrico Fermi,"* edited by W. Brandt and A. Dupasquier (Academic, New York, 1982).

<sup>2</sup>A. P. Mills, Jr., *Appl. Phys.* **23**, 189 (1980).

<sup>3</sup>A. Vehanen, K. G. Lynn, Peter J. Schultz, and M. Eldrup, *Appl. Phys. A* **32**, 2572 (1983).

<sup>4</sup>W. Cherry, Ph.D. dissertation, Princeton University, 1958 (available from University Microfilms, Inc., Ann Arbor, MI 48109).

<sup>5</sup><sup>22</sup>Na is only commercially available in a source-holder configuration that has a diameter of about 0.5 in., thus making its use difficult in a standard backscattering geometry.

<sup>6</sup>J. Van House and P. W. Zitzewitz, *Phys. Rev. A* **29**, 96 (1984).

<sup>7</sup>Peter J. Schultz, K. G. Lynn, and D. M. Chen (unpublished data).

<sup>8</sup>C. A. Murray and A. P. Mills, Jr., *Solid State Commun.* **32**, 789 (1980). See also D. Fischer, K. G. Lynn, and W. E. Frieze, *Phys. Rev. Lett.* **50**, 1149 (1983).

<sup>9</sup>Not correcting for background and grid annihilations would tend to underestimate the total reemitted yield.

<sup>10</sup>G. Mertler, M. Rey, and K. Reichelt, *Nucl. Instrum. Methods* **192**, 535 (1982).

<sup>11</sup>R. J. Wilson (private communication); A. P. Mills, Jr. and R. J. Wilson, *Phys. Rev. A* **26**, 490 (1982).

<sup>12</sup>S. Valkealahti and R. M. Nieminen, *Appl. Phys. A* **35**, 51 (1984).

<sup>13</sup>S. Valkealahti and R. M. Nieminen, *Appl. Phys. A* **32**, 95 (1983).

<sup>14</sup>A. P. Mills, Jr. and C. A. Murray, *Appl. Phys.* **21**, 323 (1980).

<sup>15</sup>R. M. Nieminen and J. Oliver, *Phys. Rev. B* **22**, 2226 (1980).

<sup>16</sup>K. G. Lynn and A. Wachs, *Appl. Phys. A* **29**, 93 (1982).

There was a numerical error in these calculations which overestimated the remoderation efficiency; see Ref. 17.

<sup>17</sup>A. Vehanen and J. Mäkinen, *Appl. Phys. A* **36**, 2902 (1985).

<sup>18</sup>Thermal positrons have wavelengths on the order of  $10^2$  Å. For very thin films of thickness compatible with the thermal positron wavelength, wave effects will dominate and the diffusion model will not be appropriate.